Inorganic Chemistry

pubs.acs.org/IC Article

Incorporation of Chromophores into Metal−Organic Frameworks for Boosting CO_2 Conversion

Yun-Nan Gong, Jin-Wang Liu, Jian-Hua Mei, Xue-Lian Lin, Ji-Hua Deng,* Xiaokang Li,* Di-Chang Zhong,* and Tong-Bu Lu

Cite This: *Inorg. Chem.* 2021, 60, 14924−14931 Read Online

ACCESS | Metrics & More | Article Recommendations | Supporting Information

ABSTRACT: The exploitation of highly stable and active catalysts for the conversion of CO_2 into valuable fuels is desirable but is a great challenge. Herein, we report that the incorporation of chromophores into metal−organic frameworks (MOFs) could afford robust catalysts for efficient CO_2 conversion. Specifically, a porous Nd(III) MOF (**Nd-TTCA**; $TTCA^{3-}$ = triphenylene-2,6,10-tricarboxylate) was constructed by incorporating one-dimensional $Nd(CO_2)_n$ chains and $TTCA^{3-}$ ligands, which exhibits a very high stability, retaining its framework not only in the air at 300 °C for 2 h but also in boiling aqueous solutions at pH 1−12 for 7 days. More importantly, **Nd-TTCA** has achieved a 5-fold improvement in photocatalytic activity for reducing CO_2 to HCOOH and a 10-fold improvement in catalytic activity for the cycloaddition of CO_2 into cyclic carbonate in comparison to those of H_3TTCA itself. This work gives a new strategy to design efficient artificial crystalline catalysts for CO_2 conversion.

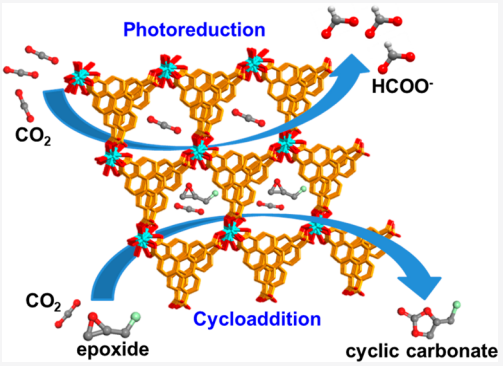

INTRODUCTION

The excessive discharge of carbon dioxide (CO_2) from the combustion of fossil fuels has caused severe environmental problems that need to be resolved urgently.[1,2] Recently, numerous approaches have been developed to efficiently store and convert CO_2.[3−10] In particular, the conversion of CO_2 into valuable fuels or other chemicals is regarded as a promising solution to alleviate the above issue. With the natural photosynthetic process as inspiration, solar-energy-driven CO_2 reduction under the action of photocatalysts into CO, HCOOH, CH_4, and so on has been extensively studied, as it is an eco-friendly means to achieve a carbon-neutral economy.[11−18] In addition, the cycloaddition of CO_2 and epoxides is another promising way to convert CO_2 into diverse fine chemicals.[19−22] However, because of the high kinetic and thermodynamic stability of CO_2 molecules, the activation of CO_2 requires a large amount of energy.[23−25] Therefore, the development of efficient artificial catalysts to activate and convert CO_2 into valuable products is highly desired.

In the past few decades, diverse homogeneous and heterogeneous catalysts have been employed for CO_2 photoreduction and cycloaddition.[26−30] Generally, homogeneous catalysts exhibit high performance but poor durability. Moreover, it is hard to isolate them from reaction systems. The incorporation of homogeneous catalysts into the heterogeneous system might overcome these shortcomings to give stable and efficient catalysts. Among the reported heterogeneous catalysts, metal−organic frameworks (MOFs) constructed by metal ions/clusters and organic ligands could be ideal models to incorporate a homogeneous molecular catalyst into a heterogeneous system.[31−43] With the unique advantages of well-defined structures, high surface area, and well-exposed active sites, MOFs have demonstrated potential in adsorbing and activating CO_2 molecules.[44−51] Furthermore, MOFs containing large conjugated organic ligands usually exhibit good light-harvesting ability and thus excellent catalytic performance. However, most MOFs exhibit poor chemical stability, which is an obstacle for them to be efficient catalysts for CO_2 conversion. To conquer this, one of the extensively accepted strategies is to construct stable MOFs by using carboxylate linkers and high-valent metals on the bsis of the hard/soft acid/base (HSAB) principle.[52−58]

Herein, we have rationally synthesized a stable Nd-carboxylate MOF (**Nd-TTCA**) by using Nd(III) ions and large conjugated tricarboxylate (H_3TTCA: triphenylene-2,6,10-tricarboxylic acid) ligands. Strikingly, **Nd-TTCA** exhibits exceptional stability, as it is not only stable in the air at 300 °C for 2 h but also robust in boiling aqueous solutions at pH 1−12 for 7 days. Photocatalytic results indicate that **Nd-TTCA** shows a 5-fold improvement in catalytic activity for reducing CO_2 to HCOOH in comparison to H_3TTCA. In

Received: July 28, 2021
Published: September 16, 2021

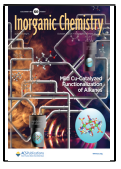

https://doi.org/10.1021/acs.inorgchem.1c02294
Inorg. Chem. 2021, 60, 14924−14931

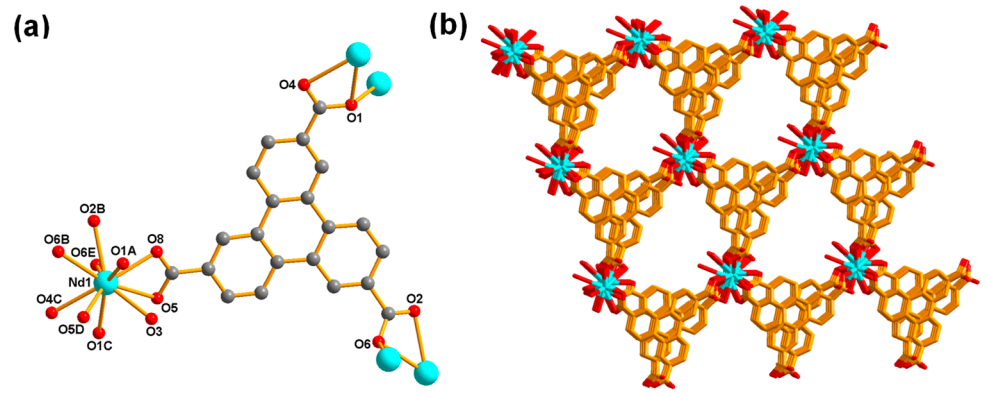

Figure 1. (a) Coordination environments of Nd(III) and $TTCA^{3-}$ in **Nd-TTCA**. Symmetry operations: (A) x, $1 - y$, $1/2 + z$; (B) $1/2 + x$, $1/2 + y$, $1 + z$; (C) x, $1 + y$, z; (D) x, $2 - y$, $1/2 + z$; (E) $1/2 + x$, $3/2 - y$, $1/2 + z$. (b) The 3D framework of **Nd-TTCA** with 1D channels.

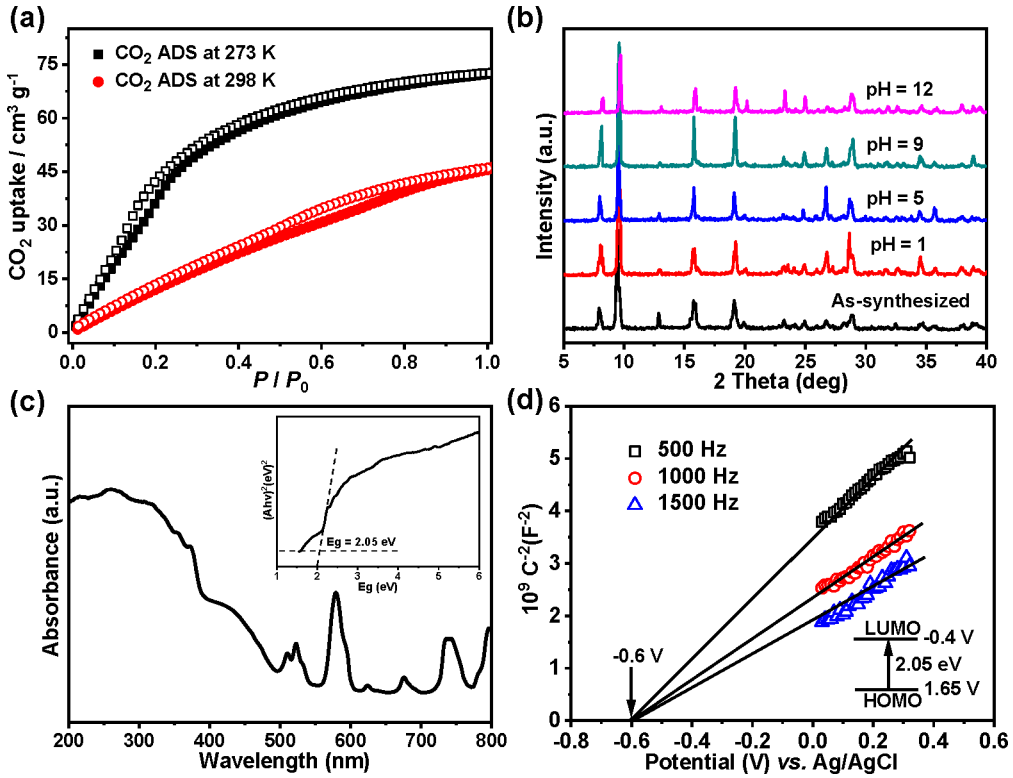

Figure 2. (a) CO_2 adsorption isotherms of **Nd-TTCA** at 273 and 298 K. (b) Powder XRD patterns of **Nd-TTCA** after treatment in boiling aqueous solutions of pH 1−12 for 7 days. (c) UV−vis spectrum and Tauc plot (inset) of **Nd-TTCA**. (d) Mott−Schottky plots for **Nd-TTCA** in 0.1 M Na_2SO_4 aqueous solution. Inset: an energy diagram of the HOMO and LUMO levels of **Nd-TTCA**.

addition, **Nd-TTCA** affords a 10-fold improvement in catalytic activity for the cycloaddition of CO_2 and glycidol in comparison to H_3TTCA. The significantly enhanced activity of **Nd-TTCA** in comparison to H_3TTCA is attributed to its rich Lewis acidic Nd(III) sites, high CO_2 capture capability, and good charge separation efficiency.

RESULTS AND DISCUSSION

The synthesis of **Nd-TTCA** was performed by the solvothermal reaction of H_3TTCA and $Nd(NO_3)_3{\cdot}6H_2O$ in *N*,*N*-dimethylformamide (DMF) at 120 °C. A single-crystal X-ray diffraction analysis indicates that **Nd-TTCA** crystallizes in the monoclinic space group *Cc* (Table S1). Each asymmetric unit contains one crystallographically independent Nd(III) ion, one $TTCA^{3-}$ ligand, one coordinated H_2O, and three-fourths of a free DMF molecule. The Nd(III) is 10-coordinated by 9 carboxylate oxygen atoms and 1 water oxygen atom (Figure 1a). The Nd−O bond lengths are in the range of 2.438−2.755 Å (Table S2). Adjacent Nd(III) ions are connected together by μ_3-CO_2 groups from $TTCA^{3-}$ ligands to generate one-dimensional (1D) $Nd(CO_2)_n$ chains (Figure S1), which are further linked by $TTCA^{3-}$ ligands to form a three-dimensional (3D) framework with 1D channels (Figure 1b). The size of the channel is 8 × 14 Å. The solvent-accessible volume within **Nd-TTCA** is 26% as calculated by PLATON.[59]

The experimental powder X-ray diffraction (XRD) pattern of **Nd-TTCA** is basically identical with the simulated pattern generated from the single-crystal diffraction data, demonstrating its high phase purity (Figure S2). The result of a thermogravimetric analysis (TGA) for **Nd-TTCA** shows a

https://doi.org/10.1021/acs.inorgchem.1c02294
Inorg. Chem. 2021, 60, 14924−14931

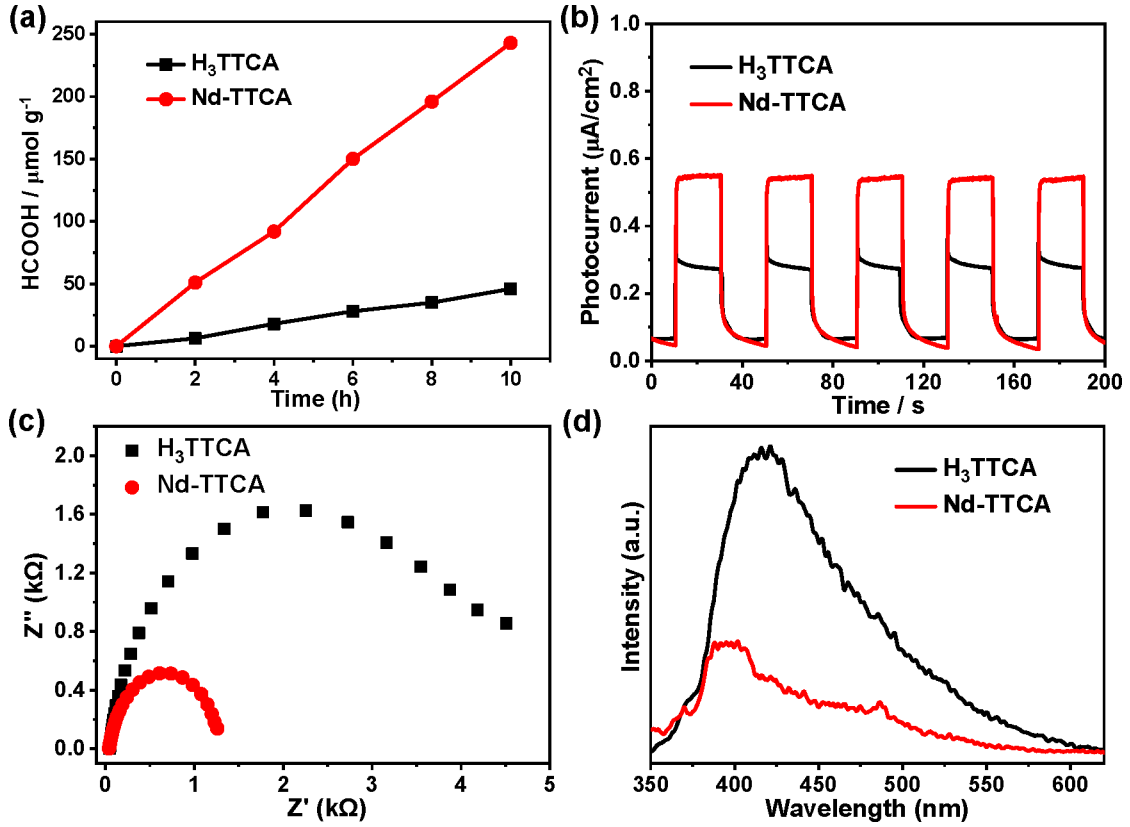

Figure 3. (a) HCOOH yield rates over **Nd-TTCA** and H_3TTCA. (b) Photocurrent tests of **Nd-TTCA** and H_3TTCA. (c) EIS plots of **Nd-TTCA** and H_3TTCA. (d) PL spectra of **Nd-TTCA** and H_3TTCA upon excitation at 330 nm.

weight loss from 30 to 280 °C, consistent with the removal of DMF and H_2O molecules. The desolvated **Nd-TTCA** exhibits high thermal stability up to 500 °C, which may be attributed to the high thermal stability of the organic ligand H_3TTCA (Figure S3). To examine the porous feature of **Nd-TTCA**, N_2 and CO_2 adsorption studies were conducted. The result of an N_2 adsorption measurement reveals a reversible type I isotherm, with a saturated N_2 adsorption capacity of 151 cm^3 g^{-1} (STP), consistent with a Brunauer−Emmett−Teller (BET) surface area of 435 m^2 g^{-1}, and a pore size distribution of 7−9 Å (Figure S4). The results of CO_2 adsorption isotherms indicate the adsorption capacities of **Nd-TTCA** are 72 cm^3 g^{-1} at 1 bar and 273 K as well as 47 cm^3 g^{-1} at 1 bar and 298 K (Figure 2a). In sharp contrast, the organic ligand H_3TTCA hardly adsorbs N_2 and CO_2 under identical conditions (Figures S5 and S6), indicating that the incorporation of the organic ligand into the porous MOF significantly enhances the gas capture capability.

In order to investigate the structural stability, **Nd-TTCA** was calcined in the air. The results of powder XRD patterns demonstrate that **Nd-TTCA** retains its structural integrity upon calcination at 300 °C for 2 h (Figure S7). The N_2 adsorption result further confirms that the framework integrity of **Nd-TTCA** is well maintained after calcination (Figure S8). Moreover, the results of powder XRD patterns demonstrate that **Nd-TTCA** shows exceptionally high stability in boiling aqueous solutions of pH 1−12 for 7 days (Figure 2b). The solid-state UV−vis spectrum of **Nd-TTCA** exhibits good light-harvesting ability in both the ultraviolet and visible regions (Figure 2c). The band-gap energy (E_g) of **Nd-TTCA** is 2.05 eV, as estimated by the Kubelka−Munk (KM) method on the basis of the UV−vis spectrum (Figure 2c). To estimate the possible semiconductor character, Mott−Schottky measurements on **Nd-TTCA** were carried out at the frequencies of 500, 1000, and 1500 Hz.[60] The C^{2-} values (vs applied potentials) of **Nd-TTCA** show a positive slope, suggesting that it is an n-type semiconductor. The flat band potential is ∼−0.60 V vs Ag/AgCl (that is, −0.40 V vs NHE), as determined by the intersection point, which is equal to the conduction band (LUMO) (Figure 2d). Thus, the valence band (HOMO) is 1.65 V vs NHE (Figure 2d). Given the more negative LUMO position for **Nd-TTCA** in comparison with that of $\varphi_{CO_2/HCOOH}$ (−0.58 V vs NHE), it can be used as a catalyst to photoreduce CO_2 to HCOOH.[60] In addition, the results of the solid-state UV−vis spectrum and Mott−Schottky measurements suggest that the H_3TTCA ligand can be used as a light-harvesting unit and an n-type semiconductor with a negative LUMO potential to photoreduce CO_2 to HCOOH (Figures S9 and S10).

From the above results, the photocatalytic reduction of CO_2 over **Nd-TTCA** and H_3TTCA were conducted under a pure CO_2 atmosphere in a mixed solution of CH_3CN and triethylamine (TEA). As shown in Table S3, **Nd-TTCA** shows good activity for the photocatalytic reduction of CO_2 to HCOOH among the various MOF catalysts. The HCOOH yield is 243 μmol g^{-1} within 10 h (Figure 3a). In sharp contrast, the HCOOH yield of H_3TTCA is only 46 μmol g^{-1} under the same conditions. The over 5 times higher photocatalytic activity of **Nd-TTCA** in comparison to that of H_3TTCA manifests that the incorporation of organic chromophores into stable MOFs is an effective strategy to enhance the photocatalytic CO_2 reduction performance.

https://doi.org/10.1021/acs.inorgchem.1c02294
Inorg. Chem. 2021, 60, 14924−14931

To confirm the photocatalytic CO_2 reduction activity of **Nd-TTCA**, some control experiments were carried out. As shown in Table S4, in the absence of CO_2, photocatalyst, TEA, or light irradiation, negligible amounts of HCOOH were detected in the photocatalytic process, prelimilarly demonstrating that the HCOOH was obtained from the photocatalytic CO_2 reduction. To further validate the carbon source origin of HCOOH, an isotopic $^{13}CO_2$ experiment was performed with the identical photocatalytic reaction.[61] The ^{13}C NMR spectrum gives the $HCOO^-$ signal at 163.3 ppm (Figures S11 and S12). This result confirms that **Nd-TTCA** is indeed active for the reduction of CO_2 to HCOOH. The photocatalytic stability of **Nd-TTCA** was evaluated by recycling experiments, which demonstrated that **Nd-TTCA** can nearly retain its initial activity during five runs (Figure S13). This result, together with the fact that there was hardly an alteration in the powder XRD patterns before and after the reactions, strongly evidences the stability of **Nd-TTCA** (Figure S14).

In order to elucidate the much higher photocatalytic activity of **Nd-TTCA** in comparison with H_3TTCA, photocurrent, electrochemical impedance spectroscopy (EIS), and photoluminescence (PL) spectra measurements of **Nd-TTCA** and H_3TTCA were carried out.[61] The results show that **Nd-TTCA** possesses a stronger photocurrent response in comparison to that of H_3TTCA (Figure 3b), revealing that the charge separation is more efficient in the former. The EIS of **Nd-TTCA** shows a smaller radius (Figure 3c), implying a lower charge-transfer resistance in comparison to H_3TTCA. PL spectra demonstrate that **Nd-TTCA** presents a pronounced PL emission quenching (Figure 3d), further illustrating increased electron transfer within **Nd-TTCA**. Moreover, the maximum PL emission peak of **Nd-TTCA** shows a 20 nm blue shift in comparison to the peak for the H_3TTCA ligand, which may be attributed to ligand to ligand charge transitions (LLCT).[62] All of these results unambiguously suggest that the incorporation of the large chromophores into **Nd-TTCA** facilitates charge separation, supporting the incremental photocatalytic CO_2 reduction activity.

To further examine the CO_2 conversion capacity, CO_2 fixation experiments of desolvated **Nd-TTCA** were carried out by the cycloaddition of CO_2 and glycidol, epichlorohydrin, or 1-bromo-2,3-epoxypropane, respectively (Table 1). Delightfully, in the presence of the cocatalyst tetrabutylammonium bromide (TBAB) and 1 bar of CO_2, **Nd-TTCA** exhibits excellent catalytic activity for these epoxides at 60 °C, with conversions of 89, 94, and 95% in 48 h, respectively (entries 1, 3, and 5). In sharp contrast, using H_3TTCA as a catalyst, only 9, 12, and 35% of glycidol, epichlorohydrin, and 1-bromo-2,3-epoxypropane were converted to the target products, respectively (entries 2, 4, and 6). **Nd-TTCA** has thus achieved about a 10-fold improvement for the conversion of glycidol in comparison to the H_3TTCA ligand. These results indicate that the incorporation of the large chromophores into **Nd-TTCA** is able to greatly boost the catalytic efficiency for the cycloaddition of CO_2 with epoxides. The significantly enhanced performance of **Nd-TTCA** might be attributed to the high CO_2 capture capability and rich Lewis acidic Nd(III) sites within **Nd-TTCA**. A recycling experiment of **Nd-TTCA** for the cycloaddition of CO_2 with glycidol was also conducted to evaluate the reaction stability and reusability. Remarkably, the conversion and selectivity of **Nd-TTCA** are well retained during the five runs of circulation (Figure 4). The powder XRD profile after the reaction is almost the same as that before the reaction (Figure S15), further confirming the excellent stability of **Nd-TTCA**.

Table 1. CO_2 Cycloaddition with Different Epoxides Catalyzed by Nd-TTCA and H_3TTCA[a]

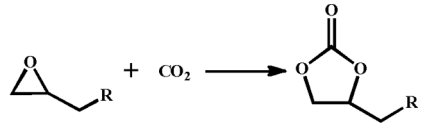

Entry	Substrate	Catalysts	Con.[b] [%]	Sel.[b] [%]
1	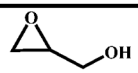	**Nd-TTCA**	89	100
2		H_3TTCA	9	100
3	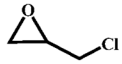	**Nd-TTCA**	94	100
4		H_3TTCA	12	100
5	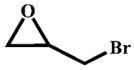	**Nd-TTCA**	95	100
6		H_3TTCA	35	100

[a]Reaction conditions: 30 μL of substrate, 50 mg of catalyst, 2 mL of acetonitrile, 30 mg of TBAB, 1 bar of CO_2, 60 °C, 48 h. [b]Determined by gas chromatography.

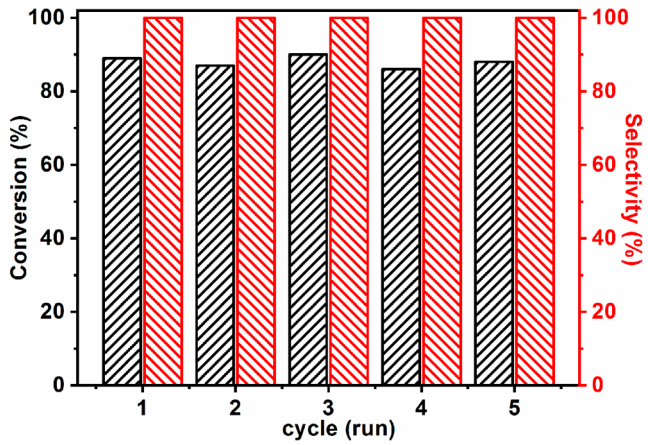

Figure 4. Conversion (black column) and selectivity (red column) of **Nd-TTCA** toward CO_2 cycloaddition with glycidol during five consecutive runs.

According to the above catalytic results, a possible mechanism for the cycloaddition of CO_2 with epoxides was proposed on the basis of previous reports.[63,64] As shown in Scheme S1, the epoxide was first adsorbed by the coordinatively unsaturated Lewis acidic Nd(III) site of activated **Nd-TTCA**. Subsequently, the less-hindered carbon atom of the epoxide was nucleophilically attacked by the bromide of TBAB, which leads to the epoxy ring opening. Then, the carbon atom of CO_2 was attacked by the ring-opened intermediate. Finally, the cyclic carbonate is generated through an intramolecular ring-closing step, followed by the regeneration of the catalyst and cocatalyst.

https://doi.org/10.1021/acs.inorgchem.1c02294
Inorg. Chem. 2021, 60, 14924−14931

CONCLUSION

In summary, by incorporation of large chromophores into a MOF framework, the resulting **Nd-TTCA** not only shows exceptional thermal and chemical stability but also exhibits a significantly increased CO_2 capture capability and charge separation efficiency. As a result, **Nd-TTCA** shows a 5-fold improvement in photocatalytic activity for reducing CO_2 to HCOOH and a 10-fold improvement in catalytic activity for the cycloaddition of CO_2 and glycidol in comparison to the H_3TTCA ligand. This work provides a new method for the exploitation of stable and efficient catalysts for CO_2 conversion.

EXPERIMENTAL SECTION

Materials and Instrumentation. All chemicals were commercially available and were used without further purification. H_3TTCA was synthesized according to the literature.[65] Powder XRD patterns were recorded on Japan Rigaku Miniflex 600 rotation anode and D8 ADVANCE X-ray diffractometers with Cu Kα radiation (λ = 1.54 Å). Elemental analyses were conducted using an Elementar Vario EL elemental analyzer. TGA was performed on Netzsch TG-209 Thermogravimetry Analyzer. Gas sorption experiments were carried out using Micromeritics ASAP 2020 and Microtrac BEL BELSORP-Mas systems. UV−vis spectra were determined with a Shimadzu UV-2700 spectrophotometer. PL spectral measurements were performed using an LS-55 fluorescence spectrometer. $HCOO^-$ was analyzed using ^{13}C nuclear magnetic resonance (NMR, Bruker AVANCE AV III 400) spectroscopy and ion chromatography (CASTLE C1K-3K UPS). The products of CO_2 cycloaddition were determined using a Shimadzu gas chromatograph (GC-2010 Plus with a 0.25 mm × 30 m Rtx-5 capillary column).

Synthesis of $[Nd_4(TTCA)_4(H_2O)_4]\cdot 3DMF$ (Nd-TTCA). A sealed Teflon-lined autoclave containing a mixture of $Nd(NO_3)_3\cdot 6H_2O$ (0.044 g, 0.1 mmol), H_3TTCA (0.018 g, 0.05 mmol), DMF (8.0 mL), and hydrochloric acid (1 drop) was heated at 120 °C for 48 h. Then the autoclave was cooled to 25 °C. Lilac block-shaped crystals of **Nd-TTCA** were obtained by filtration. Yield: 45%. Anal. Calcd for $C_{93}H_{65}N_3O_{31}Nd_4$ (**Nd-TTCA**): C, 48.62; H, 2.85; N, 1.83. Found: C, 48.12; H, 3.22; N, 2.14.

X-ray Crystallography. The single-crystal data of **Nd-TTCA** were collected using an Agilent Technologies Gemini A Ultra system, with Cu Kα radiation (λ = 1.54 Å). The structure of **Nd-TTCA** was solved and refined by using SHELXT within the OLEX2 graphical interface.[66−68] All non-hydrogen atoms were refined isotropically and followed anisotropically. All of the hydrogen atoms were placed in calculated positions with fixed isotropic thermal parameters and included in the structure factor calculations in the final stage of full-matrix least-squares refinement. The crystallographic data of **Nd-TTCA** are summarized in Table S1, and selected bond lengths and angles are given in Table S2.

Photocatalytic Experiments. A photoreactor (25 mL) containing the photocatalyst (20 mg), triethylamine (TEA, 0.5 mL), and acetonitrile (CH_3CN, 10 mL) was degassed with CO_2 to remove O_2 and other gases, followed by 300 W Xe lamp (CEL-HXF300, CEAULICHT) irradiation with the full spectrum. $HCOO^-$ was analyzed by ion chromatography and ^{13}C NMR spectroscopy.

Catalytic Cycloaddition of CO_2 and Epoxide. A round-bottom flask (5 mL) containing the catalyst (50 mg), TBAB (30 mg), CH_3CN (2 mL), and epoxide (30 μL) was connected to a CO_2 balloon. Then the reaction mixture was stirred at 60 °C for 48 h. After that, the catalysts were separated by centrifugation, and the liquid products were analyzed using gas chromatography to determine the conversions.

Photoelectrochemical Measurements. Photocurrent measurements were performed using a CHI 760E electrochemical workstation with a standard three-electrode system in 0.1 M Na_2SO_4 solution. Photocatalyst-coated FTO, a platinum plate, and a saturated Ag/AgCl were used as working, counter, and reference electrodes, respectively. A 300 W Xe lamp with a full spectrum was used as the light source. **Nd-TTCA** or H_3TTCA (5 mg) was dispersed into 0.5 mL of ethanol containing 10 μL of Nafion. The working electrodes were prepared by depositing 60 μL of the mixture onto an FTO plate with an area of 4 cm^2. Photoresponsive signals of **Nd-TTCA** and H_3TTCA were measured under chopped light at +0.6 V.

EIS and Mott−Schottky plots of **Nd-TTCA** and H_3TTCA in 0.1 M Na_2SO_4 aqueous solution were determined on a Zahner Zennium electrochemical workstation. Photocatalyst-coated glassy carbon (Φ = 3 cm), a platinum plate, and a saturated Ag/AgCl were used as the working, counter, and reference electrodes, respectively. **Nd-TTCA** or H_3TTCA (5 mg) was dispersed into 0.5 mL of ethanol containing 10 μL of Nafion. Then 30 μL of the mixture was deposited onto the glassy-carbon electrode. EIS measurement was carried out using a bias potential of −1.6 V in the dark. Mott−Schottky plots were recorded at frequencies of 500, 1000, and 1500 Hz, respectively.

ASSOCIATED CONTENT

Supporting Information

The Supporting Information is available free of charge at https://pubs.acs.org/doi/10.1021/acs.inorgchem.1c02294.

Crystallographic data, photocatalytic results, crystal structure, powder XRD patterns, TGA curves, gas sorption isotherms, UV−vis spectrum, Mott−Schottky plots, ^{13}C NMR spectra, recycling experiments, and proposed mechanism (PDF)

Accession Codes

CCDC 2064450 contains the supplementary crystallographic data for this paper. These data can be obtained free of charge via www.ccdc.cam.ac.uk/data_request/cif, or by emailing data_request@ccdc.cam.ac.uk, or by contacting The Cambridge Crystallographic Data Centre, 12 Union Road, Cambridge CB2 1EZ, UK; fax: +44 1223 336033.

AUTHOR INFORMATION

Corresponding Authors

Ji-Hua Deng − *Institute for New Energy Materials and Low Carbon Technologies, School of Materials Science and Engineering, School of Chemistry and Chemical Engineering, Tianjin University of Technology, Tianjin 300384, People's Republic of China*; Email: djhycu_2006@aliyun.com

Xiaokang Li − *Key Laboratory of Jiangxi University for Functional Material Chemistry, College of Chemistry & Chemical Engineering, Gannan Normal University, Ganzhou 341000, People's Republic of China*; Email: gnnulxk@163.com

Di-Chang Zhong − *Institute for New Energy Materials and Low Carbon Technologies, School of Materials Science and Engineering, School of Chemistry and Chemical Engineering, Tianjin University of Technology, Tianjin 300384, People's Republic of China*; orcid.org/0000-0002-5504-249X; Email: dczhong@email.tjut.edu.cn

Authors

Yun-Nan Gong − *Institute for New Energy Materials and Low Carbon Technologies, School of Materials Science and Engineering, School of Chemistry and Chemical Engineering, Tianjin University of Technology, Tianjin 300384, People's Republic of China*

Jin-Wang Liu − *Key Laboratory of Jiangxi University for Functional Material Chemistry, College of Chemistry & Chemical Engineering, Gannan Normal University, Ganzhou 341000, People's Republic of China*

Jian-Hua Mei − *Institute for New Energy Materials and Low Carbon Technologies, School of Materials Science and Engineering, School of Chemistry and Chemical Engineering, Tianjin University of Technology, Tianjin 300384, People's Republic of China*

Xue-Lian Lin − *Key Laboratory of Jiangxi University for Functional Material Chemistry, College of Chemistry & Chemical Engineering, Gannan Normal University, Ganzhou 341000, People's Republic of China*

Tong-Bu Lu − *Institute for New Energy Materials and Low Carbon Technologies, School of Materials Science and Engineering, School of Chemistry and Chemical Engineering, Tianjin University of Technology, Tianjin 300384, People's Republic of China;* orcid.org/0000-0002-6087-4880

Complete contact information is available at: https://pubs.acs.org/10.1021/acs.inorgchem.1c02294

Notes

The authors declare no competing financial interest.

■ ACKNOWLEDGMENTS

This work was supported by the National Natural Science Foundation of China (21861001, 21931007, 21962002, 22001043, 22071182), the National Key R&D Program of China (2017YFA0700104), the Natural Science Foundation of Jiangxi Province (20202BAB203001), the Science Foundation of the Jiangxi Provincial Office of Education (GJJ190753), the 111 Project of China (D17003), and the Science & Technology Development Fund of Tianjin Education Commission for Higher Education (2018KJ129).

■ REFERENCES

(1) Shakun, J. D.; Clark, P. U.; He, F.; Marcoot, S. A.; Mix, A. C.; Liu, Z.; Otto-Bliesner, B.; Schmittner, A.; Bard, E. Global warming preceded by increasing carbon dioxide concentrations during the last deglaciation. *Nature* **2012**, *484*, 49−54.

(2) Goeppert, A.; Czaun, M.; Jones, J.-P.; Prakash, G. K. S.; Olah, G. A. Recycling of carbon dioxide to methanol and derived products-closing the loop. *Chem. Soc. Rev.* **2014**, *43*, 7995−8048.

(3) Marques Mota, F.; Kim, D. H. From CO_2 methanation to ambitious long chain hydrocarbons: alternative fuels paving the path to sustainability. *Chem. Soc. Rev.* **2019**, *48*, 205−259.

(4) Ding, M.; Flaig, R. W.; Jiang, H.-L.; Yaghi, O. M. Carbon capture and conversion using metal-organic frameworks and MOF-based materials. *Chem. Soc. Rev.* **2019**, *48*, 2783−2828.

(5) Hou, Y.; Huang, Y.-B.; Liang, Y.-L.; Chai, G.-L.; Yi, J.-D.; Zhang, T.; Zang, K.-T.; Luo, J.; Xu, R.; Lin, H.; Zhang, S.-Y.; Wang, H.-M.; Cao, R. Unraveling the reactivity and selectivity of atomically isolated metal-nitrogen sites anchored on porphyrinic triazine frameworks for electroreduction of CO_2. *CCS Chem.* **2019**, *1*, 384−395.

(6) Ran, J.; Jaroniec, M.; Qiao, S.-Z. Cocatalysts in semiconductor based photocatalytic CO_2 reduction: achievements, challenges, and opportunities. *Adv. Mater.* **2018**, *30*, 1704649.

(7) Wang, Y.-R.; Huang, Q.; He, C.-T.; Chen, Y.; Liu, J.; Shen, F.-C.; Lan, Y.-Q. Oriented electron transmission in polyoxometalate-metalloporphyrin organic framework for highly selective electroreduction of CO_2. *Nat. Commun.* **2018**, *9*, 4466.

(8) Zhang, L.; Zhao, Z.-J.; Wang, T.; Gong, J. Nano-designed semiconductors for electro- and photoelectro-catalytic conversion of carbon dioxide. *Chem. Soc. Rev.* **2018**, *47*, 5423−5443.

(9) Rong, X.; Wang, H.-J.; Lu, X.-L.; Si, R.; Lu, T.-B. Controlled synthesis of a vacancy-defect single-atom catalyst for boosting CO_2 electroreduction. *Angew. Chem., Int. Ed.* **2020**, *59*, 1961−1965.

(10) Zhang, B.; Zhao, T.-J.; Feng, W.-J.; Liu, Y.-X.; Wang, H.-H.; Su, H.; Lv, L.-B.; Li, X.-H.; Chen, J.-S. Polarized few-layer g-C_3N_4 as metal-free electrocatalyst for highly efficient reduction of CO_2. *Nano Res.* **2018**, *11*, 2450−2459.

(11) Yi, J.-D.; Xie, R.; Xie, Z.-L.; Chai, G.-L.; Liu, T.-F.; Chen, R.-P.; Huang, Y.-B.; Cao, R. Highly selective CO_2 electroreduction to CH_4 by in situ generated Cu_2O single-type sites on a conductive MOF: stabilizing key intermediates with hydrogen bonding. *Angew. Chem., Int. Ed.* **2020**, *59*, 23641−23648.

(12) Li, D.; Kassymova, M.; Cai, X.; Zang, S.-Q.; Jiang, H.-L. Photocatalytic CO_2 reduction over metal-organic framework-based materials. *Coord. Chem. Rev.* **2020**, *412*, 213262.

(13) Liu, D. C.; Zhong, D. C.; Lu, T.-B. Non-noble metal-based molecular complexes for CO_2 reduction: from the ligand design perspective. *EnergyChem.* **2020**, *2*, 100034.

(14) Kong, T.; Jiang, Y.; Xiong, Y. Photocatalytic CO_2 conversion: What can we learn from conventional CO_x hydrogenation? *Chem. Soc. Rev.* **2020**, *49*, 6579−6591.

(15) Chen, Y.; Wang, D.; Deng, X.; Li, Z. Metal-organic frameworks (MOFs) for photocatalytic CO_2 reduction. *Catal. Sci. Technol.* **2017**, *7*, 4893−4904.

(16) Yang, W.; Wang, H.-J.; Liu, R.-R.; Wang, J.-W.; Zhang, C.; Li, C.; Zhong, D.-C.; Lu, T.-B. Tailoring crystal facets of metal-organic layers to enhance photocatalytic activity for CO_2 reduction. *Angew. Chem., Int. Ed.* **2021**, *60*, 409−414.

(17) Meng, S.; Chen, C.; Gu, X.; Wu, H.; Meng, Q.; Zhang, J.; Chen, S.; Fu, X.; Liu, D.; Lei, W. Efficient photocatalytic H2 evolution, CO_2 reduction and N_2 fixation coupled with organic synthesis by cocatalyst and vacancies engineering. *Appl. Catal., B* **2021**, *285*, 119789.

(18) Deng, X.; Qin, Y.; Hao, M.; Li, Z. MOF-253-supported Ru complex for photocatalytic CO_2 reduction by coupling with semidehydrogenation of 1,2,3,4-Tetrahydroisoquinoline (THIQ). *Inorg. Chem.* **2019**, *58*, 16574−16580.

(19) He, H.; Perman, J. A.; Zhu, G.; Ma, S. Metal-organic frameworks for CO_2 chemical transformations. *Small* **2016**, *12*, 6309−6324.

(20) Zou, Y.-H.; Wu, Q.-J.; Yin, Q.; Huang, Y.-B.; Cao, R. Self-assembly of imidazolium-functionalized Zr-based metal-organic polyhedra for catalytic conversion of CO_2 into cyclic carbonates. *Inorg. Chem.* **2021**, *60*, 2112−2116.

(21) Lu, X.-B.; Darensbourg, D. J. Cobalt catalysts for the coupling of CO_2 and epoxides to provide polycarbonates and cyclic carbonates. *Chem. Soc. Rev.* **2012**, *41*, 1462−1484.

(22) Ding, M.; Chen, S.; Liu, X.-Q.; Sun, L.-B.; Lu, J.; Jiang, H.-L. Metal-organic framework-templated catalyst: synergy in multiple sites for catalytic CO_2 fixation. *ChemSusChem* **2017**, *10*, 1898−1903.

(23) Liang, J.; Chen, R.-P.; Wang, X.-Y.; Liu, T.-T.; Wang, X.-S.; Huang, Y.-B.; Cao, R. Postsynthetic ionization of an imidazole-containing metal-organic framework for the cycloaddition of carbon dioxide and epoxides. *Chem. Sci.* **2017**, *8*, 1570−1575.

(24) Qiao, J.; Liu, Y.; Hong, F.; Zhang, J. A review of catalysts for the electroreduction of carbon dioxide to produce low-carbon fuels. *Chem. Soc. Rev.* **2014**, *43*, 631−675.

(25) Song, C. Global challenges and strategies for control, conversion and utilization of CO_2 for sustainable development involving energy, catalysis, adsorption and chemical processing. *Catal. Today* **2006**, *115*, 2−32.

(26) Decortes, A.; Castilla, A. M.; Kleij, A. W. Salen-complex mediated formation of cyclic carbonates by cycloaddition of CO_2 to epoxides. *Angew. Chem., Int. Ed.* **2010**, *49*, 9822−9837.

(27) Wang, J.-W.; Liu, W.-J.; Zhong, D.-C.; Lu, T.-B. Nickel complexes as molecular catalysts for water splitting and CO_2 reduction. *Coord. Chem. Rev.* **2019**, *378*, 237−261.

(28) Dong, L.-Z.; Zhang, L.; Liu, J.; Huang, Q.; Lu, M.; Ji, W.-X.; Lan, Y.-Q. Stable heterometallic cluster-based organic frameworks catalysts for artificial photosynthesis. *Angew. Chem., Int. Ed.* **2020**, *59*, 2659−2663.

(29) Jiang, Z.; Xu, X.; Ma, Y.; Cho, H. S.; Ding, D.; Wang, C.; Wu, J.; Oleynikov, P.; Jia, M.; Cheng, J.; Zhou, Y.; Terasaki, O.; Peng, T.;

Zan, L.; Deng, H. Filling metal−organic framework mesopores with TiO_2 for CO_2 photoreduction. *Nature* **2020**, *586*, 549−554.
(30) Liu, W.; Li, X.; Wang, C.; Pan, H.; Liu, W.; Wang, K.; Zeng, Q.; Wang, R.; Jiang, J. A scalable general synthetic approach toward ultrathin imine-linked two-dimensional covalent organic framework nanosheets for photocatalytic CO_2 reduction. *J. Am. Chem. Soc.* **2019**, *141*, 17431−17440.
(31) Zhou, H.-C.; Kitagawa, S. Metal-organic frameworks (MOFs). *Chem. Soc. Rev.* **2014**, *43*, 5415−5148.
(32) Liao, W.-M.; Zhang, J.-H.; Yin, S.-Y.; Lin, H.; Zhang, X.; Wang, J.; Wang, H.-P.; Wu, K.; Wang, Z.; Fan, Y.-N.; Pan, M.; Su, C.-Y. Tailoring exciton and excimer emission in an exfoliated ultrathin 2D metal-organic framework. *Nat. Commun.* **2018**, *9*, 2401.
(33) Deng, J.-H.; Wen, Y.-Q.; Willman, J.; Liu, W.-J.; Gong, Y.-N.; Zhong, D.-C.; Lu, T.-B.; Zhou, H.-C. Facile exfoliation of 3D pillared metal-organic frameworks (MOFs) to produce MOF nanosheets with functionalized surfaces. *Inorg. Chem.* **2019**, *58*, 11020−11027.
(34) Zhang, X.; Wang, B.; Alsalme, A.; Xiang, S.; Zhang, Z.; Chen, B. Design and applications of water-stable metal-organic frameworks: status and challenges. *Coord. Chem. Rev.* **2020**, *423*, 213507.
(35) Zou, Y.-H.; Huang, Y.-B.; Si, D.-H.; Yin, Q.; Wu, Q.-J.; Weng, Z.; Cao, R. Porous metal-organic framework liquids for enhanced CO_2 adsorption and catalytic conversion. *Angew. Chem.* **2021**, *133*, 21083−21088.
(36) Wang, Y.; Feng, L.; Fan, W.; Wang, K.-Y.; Wang, X.; Wang, X.; Zhang, K.; Zhang, X.; Dai, F.; Sun, D.; Zhou, H.-C. Topology exploration in highly connected rare-earth metal-organic frameworks via continuous hindrance control. *J. Am. Chem. Soc.* **2019**, *141*, 6967−6975.
(37) Liu, D.; Wan, J.; Pang, G.; Tang, Z. Hollow metal-organic framework micro/nanostructures and their derivatives: emerging multifunctional materials. *Adv. Mater.* **2019**, *31*, 1803291.
(38) Zhao, X.; Wang, Y.; Li, D.-S.; Bu, X.; Feng, P. Metal-organic frameworks for separation. *Adv. Mater.* **2018**, *30*, 1705189.
(39) Gong, Y.-N.; Mei, J.-H.; Liu, J.-W.; Huang, H.-H.; Zhang, J.-H.; Li, X.; Zhong, D.-C.; Lu, T.-B. Manipulating metal oxidation state over ultrastable metal-organic frameworks for boosting photocatalysis. *Appl. Catal., B* **2021**, *292*, 120156.
(40) Hou, C.; Zhao, G.; Ji, Y.; Niu, Z.; Wang, D.; Li, Y. Hydroformylation of alkenes over rhodium supported on the metal-organic framework ZIF-8. *Nano Res.* **2014**, *7*, 1364−1369.
(41) Xiong, W.; Li, H.; You, H.; Cao, M.; Cao, R. Encapsulating metal organic framework into hollow mesoporous carbon sphere as efficient oxygen bifunctional electrocatalyst. *Natl. Sci. Rev.* **2020**, *7*, 609−619.
(42) Gong, Y.-N.; Wei, X.-W.; He, L.-H.; Wen, Y.-Q.; Ren, Y.-W.; Xie, Y.-R.; Zhong, D.-C. Two bilayer metal−organic frameworks with rare trinuclear heterometal clusters and tunable photoluminescence. *Dalton Trans.* **2017**, *46*, 7403−7407.
(43) Wang, C.; Zhang, L.; Wang, J.-Y.; Su, S.; Jin, X.-W.; An, P.-J.; Sun, B.-W.; Luo, Y.-H. Ultra-thin two-dimensional nanosheets for in-situ NIR light-triggered fluorescence enhancement. *FlatChem.* **2020**, *24*, 100193.
(44) Yi, J.-D.; Si, D.-H.; Xie, R.; Yin, Q.; Zhang, M.-D.; Wu, Q.; Chai, G.-L.; Huang, Y.-B.; Cao, R. Conductive two-dimensional phthalocyanine-based metal-organic framework nanosheets for efficient electroreduction of CO_2. *Angew. Chem., Int. Ed.* **2021**, *60*, 17108−17114.
(45) Xu, G.; Zhang, H.; Wei, J.; Zhang, H.-X.; Wu, X.; Li, Y.; Li, C.; Zhang, J.; Ye, J. Integrating g-C_3N_4 nanosheet with B-H bonding decorated metal-organic framework for CO_2 activation and photoreduction. *ACS Nano* **2018**, *12*, 5333−5340.
(46) Wang, Y.; Huang, N.-Y.; Shen, J.-Q.; Liao, P.-Q.; Chen, X.-M.; Zhang, J.-P. Hydroxide ligands cooperate with catalytic centers in metal-organic frameworks for efficient photocatalytic CO_2 reduction. *J. Am. Chem. Soc.* **2018**, *140*, 38−41.
(47) Li, X.; Zhu, Q.-L. MOF-based materials for photo- and electrocatalytic CO_2 reduction. *EnergyChem.* **2020**, *2*, 100033.
(48) Wang, X.; Gao, W.-Y.; Niu, Z.; Wojtas, L.; Perman, J. A.; Chen, Y.-S.; Li, Z.; Aguila, B.; Ma, S. A metal-metalloporphyrin framework based on an octatopicporphyrin ligand for chemical fixation of CO_2 with a ziridines. *Chem. Commun.* **2018**, *54*, 1170−1173.
(49) Tong, H.-Y.; Liang, J.; Wu, Q.-J.; Zou, Y.-H.; Huang, Y.-B.; Cao, R. Soluble imidazolium-functionalized coordination cages for efficient homogeneous catalysis of CO_2 cycloaddition reactions. *Chem. Commun.* **2021**, *57*, 2140−2143.
(50) Fan, W.; Yuan, S.; Wang, W.; Feng, L.; Liu, X.; Zhang, X.; Wang, X.; Kang, Z.; Dai, F.; Yuan, D.; Sun, D.; Zhou, H.-C. Optimizing multivariate metal-organic frameworks for efficient C_2H_2/CO_2 separation. *J. Am. Chem. Soc.* **2020**, *142*, 8728−8737.
(51) Gong, Y.-N.; Xiong, P.; He, C.-T.; Deng, J.-H.; Zhong, D.-C. A lanthanum carboxylate framework with exceptional stability and highly selective adsorption of gas and liquid. *Inorg. Chem.* **2018**, *57*, 5013−5018.
(52) Burtch, N. C.; Jasuja, H.; Walton, K. S. Water stability and adsorption in metal-organic frameworks. *Chem. Rev.* **2014**, *114*, 10575−10612.
(53) Chen, C.-X.; Wei, Z.-W.; Fan, Y.-N.; Su, P.-Y.; Ai, Y.-Y.; Qiu, Q.-F.; Wu, K.; Yin, S.-Y.; Pan, M.; Su, C.-Y. Visualization of anisotropic and stepwise piezofluorochromism in an MOF single crystal. *Chem.* **2018**, *4*, 2658−2669.
(54) Yuan, S.; Feng, L.; Wang, K.; Pang, J.; Bosch, M.; Lollar, C.; Sun, Y.; Qin, J.; Yang, X.; Zhang, P.; Wang, Q.; Zou, L.; Zhang, Y.; Zhang, L.; Fang, Y.; Li, J.; Zhou, H.-C. Stable metal-organic frameworks: design, synthesis, and applications. *Adv. Mater.* **2018**, *30*, 1704303.
(55) Gong, Y.-N.; Ouyang, T.; He, C.-T.; Lu, T.-B. Photoinduced water oxidation by an organic ligand incorporated into the framework of a stable metal-organic framework. *Chem. Sci.* **2016**, *7*, 1070−1075.
(56) Fateeva, A.; Chater, P. A.; Ireland, C. P.; Tahir, A. A.; Khimyak, Y. Z.; Wiper, P. V.; Darwent, J. R.; Rosseinsky, M. J. A water-stable porphyrin-based metal-organic framework active for visible-light photocatalysis. *Angew. Chem., Int. Ed.* **2012**, *51*, 7440−7444.
(57) Gong, Y.-N.; Liu, J.-W.; Shao, B.-Z.; Zhong, D.-C.; Lu, T.-B. Stable metal-organic frameworks for PEC water splitting. *FlatChem.* **2021**, *27*, 100240.
(58) Chen, C.-X.; Yin, S.-Y.; Wei, Z.-W.; Qiu, Q.-F.; Zhu, N.-X.; Fan, Y.-N.; Pan, M.; Su, C.-Y. Pressure-induced multiphoton excited fluorochromic metal-organic frameworks for improving MPEF properties. *Angew. Chem., Int. Ed.* **2019**, *58*, 14379−14385.
(59) Spek, A. L. *PLATON 99: A multipurpose crystallographic tool*; Utrecht University: 1999.
(60) Li, N.; Liu, J.; Liu, J.-J.; Dong, L.-Z.; Xin, Z.-F.; Teng, Y. L.; Lan, Y.-Q. Adenine components in biomimetic metal-organic frameworks for efficient CO_2 photoconversion. *Angew. Chem., Int. Ed.* **2019**, *58*, 5226−5231.
(61) Gong, Y.-N.; Zhong, W.; Li, Y.; Qiu, Y.; Zheng, L.; Jiang, J.; Jiang, H.-L. Regulating photocatalysis by spin-state manipulation of cobalt in covalent organic frameworks. *J. Am. Chem. Soc.* **2020**, *142*, 16723−16731.
(62) Gong, Y.-N.; Xie, Y.-R.; Zhong, D.-C.; Du, Z.-Y.; Lu, T.-B. A two-fold interpenetrating porous metal-organic framework with a large solvent-accessible volume: gas sorption and luminescent properties. *Cryst. Growth Des.* **2015**, *15*, 3119−3122.
(63) Wei, N.; Zhang, Y.; Liu, L.; Han, Z.-B.; Yuan, D.-Q. Pentanuclear Yb(III) cluster-based metal-organic frameworks as heterogeneous catalysts for CO_2 conversion. *Appl. Catal., B* **2017**, *219*, 603−610.
(64) Liang, J.; Xie, Y.-Q.; Wu, Q.; Wang, X.-Y.; Liu, T.-T.; Li, H.-F.; Huang, Y.-B.; Cao, R. Zinc porphyrin/imidazolium integrated multivariate zirconium metal-organic frameworks for transformation of CO_2 into cyclic carbonates. *Inorg. Chem.* **2018**, *57*, 2584−2593.
(65) Gong, Y. N.; Meng, M.; Zhong, D. C.; Huang, Y. L.; Jiang, L.; Lu, T.-B. Counter-cation modulation of hydrogen and methane storage in a sodalite-type porous metal-organic framework. *Chem. Commun.* **2012**, *48*, 12002−12004.

https://doi.org/10.1021/acs.inorgchem.1c02294
Inorg. Chem. 2021, 60, 14924−14931

(66) Sheldrick, G. M. SHELXT-Integrated space-group and crystal structure determination. *Acta Crystallogr., Sect. A: Found. Adv.* **2015**, *71*, 3−8.
(67) Sheldrick, G. M. Crystal structure refinement with SHLEXL. *Acta Crystallogr., Sect. A: Found. Adv.* **2015**, *71*, 3−8.
(68) Dolomanov, O. V.; Bourhis, L. J.; Gildea, R. J.; Howard, J. A. K.; Puschmann, H. OLEX2: A complete structure solution, refinement and analysis program. *J. Appl. Crystallogr.* **2009**, *42*, 339−341.

https://doi.org/10.1021/acs.inorgchem.1c02294
Inorg. Chem. 2021, 60, 14924−14931